JOURNAL OF CATALYSIS 87, 55–65 (1984)

Effects of Support on Hydrogen Adsorption/Desorption Kinetics of Nickel

GORDON D. WEATHERBEE AND CALVIN H. BARTHOLOMEW

BYU Catalysis Laboratory, Department of Chemical Engineering, Brigham Young University, Provo, Utah 84602

Received May 6, 1983; revised December 8, 1983

Kinetics and energetics of hydrogen adsorption on unsupported nickel and nickel supported on silica, alumina, and titania were investigated by means of temperature-programmed desorption. The number and population of adsorption states at moderate to low coverages and heats of adsorption were found to be strong functions of the support. Heats of adsorption ranged from approximately 85 kJ/mole on unsupported Ni and Ni/SiO_2 to 122 kJ/mole on Ni/Al_2O_3. In addition, hydrogen adsorption on Ni/Al_2O_3 was found to be an activated process. Reduction of Ni/TiO_2 at high temperatures (600–700°C) was observed to strongly suppress the adsorption of hydrogen and shift the TPD spectrum to lower binding energies. Desorption spectra obtained using an N_2 carrier gas were significantly different from those obtained using Ar or He carrier gases probably due to competitive adsorption of N_2 on the nickel surface.

INTRODUCTION

Although effects of support on the adsorption properties of nickel were reported over 2 decades ago (*1*), there has been significant emphasis on their study only during the past 4–5 years. Several recent studies (*2–7*) provide evidence that metal–support interactions markedly influence H_2 and CO adsorption properties of nickel. For example, studies by Bartholomew *et al.* (*3–4*) and Vannice *et al.* (*2, 5*) provide evidence that CO adsorption stoichiometries are greatly modified by strong metal–support interactions in well-dispersed Ni/SiO_2 and moderately dispersed Ni/Al_2O_3 and Ni/TiO_2 catalysts. Moreover, H_2 adsorption is suppressed at low loadings in Ni/Al_2O_3 and at moderate loadings in Ni/TiO_2 (*3*). The stoichiometry of O_2 adsorption is also different on Ni/TiO_2 compared to Ni/SiO_2 and Ni/Al_2O_3 (*5*). Finally, from temperature-programmed desorption (TPD) studies by Falconer *et al.* (*6, 7*) the kinetics of CO and CO_2 desorption as well as CO and CO_2 adsorption states have been found to differ greatly for Ni/Al_2O_3 and Ni/SiO_2.

TPD spectroscopy of catalysts is an outgrowth of flash desorption spectroscopy originally developed for single crystal and polycrystalline metals. The early application of TPD to catalysts was described by Cvetanovic and Amenomiya (*8, 9*), while more recently developed techniques and recent studies were reviewed by Falconer and Schwarz (*10*). The quantitative application of TPD to the study of H_2 desorption kinetics on Ni/SiO_2 was recently demonstrated by Lee and Schwarz (*11*).

While numerous previous TPD studies of H_2 from single crystal nickel have been reported (*12*), relatively few TPD studies of hydrogen from supported nickel have been published (*11, 13,14*), most of which focused on the Ni/SiO_2 system (*11, 14*). At the time this study was undertaken there had been no previous systematic investigation of H_2 desorption from supported nickel to determine effects of support. The purpose of this investigation was therefore to determine the effects of SiO_2, Al_2O_3, and TiO_2 supports on (i) the H_2 adsorption states of nickel and (ii) the binding energy of H_2 with nickel.

0021-9517/84 $3.00

EXPERIMENTAL

The 3% Ni/SiO_2, 10% Ni/SiO_2, 14% Ni/Al_2O_3, and 10% Ni/TiO_2 catalysts were prepared by aqueous impregnation of the support followed by oven drying and *in situ* reduction in flowing H_2. Details of the preparation and characterization of these catalysts were provided previously (*3, 4, 15, 16*). During reduction of these catalysts a temperature ramp of 2°C/min to 200°C, a 2-h hold, and 2°C/min ramp to 500°C with a 16-h hold were used (*15*). A 50 wt% Ni/SiO_2 catalyst was supplied by Dr. J. L. Carter of Exxon Research and Engineering; its properties are described by Lee and Schwarz (*11*). Unsupported Ni powder (INCO) was prepared by direct reduction of the nitrate salt in flowing hydrogen using a temperature schedule similar to that given above but with a maximum temperature of 400°C to avoid sintering.

Ultrahigh purity N_2 (99.999%), Ar (99.999%), and He (99.999%) from Linde Division, Union Carbide, were passed through a Matheson Gas purifier, heated Ni and Cu traps and molecular sieve (Linde Type 5A) to remove H_2O and O_2 impurities. Hydrogen (99.99%) was further purified by passing through a Pt/Pd Deoxo unit and molecular sieve (Linde Type 5A) traps.

The reactor consisted of a 6.4-mm o.d./4-mm i.d. quartz tube. Small, loosely packed plugs of quartz wool were used to support the catalyst in the tube. The reactor tube was housed inside a tubular oven with a 14-cm-long heated section which produced a uniform temperature profile along the catalyst bed. An unshielded Chromel–Alumel thermocouple was placed in contact with the oven wall in the annular space between the oven and the reactor tube to provide input signals for the temperature controller. A second stainless-steel shielded Chromel–Alumel thermocouple was placed inside the reactor tube to measure the bed temperature. Oven temperature was controlled with a programmable temperature controller designed and constructed inhouse.

A Carle Instruments 6-port gas sampling valve with 0.1-cm^3 sample loop was used to inject pulses of 10% H_2 in Ar, N_2, or He into the carrier gas stream for adsorption on the catalyst sample. Carrier gas flow rates were controlled by two-stage regulators and Brooks gas chromatograph flow-control valves. A Hewlett–Packard 5730A gas chromatograph thermal conductivity detector (TCD) or a UTI 100C mass spectrometer was used to analyze the H_2 concentration during adsorption and desorption experiments.

Previously reduced and passivated catalyst samples of 15 to 50 mg were loaded into the reactor and heated slowly in H_2 to 500°C and held for 2 h. The reactor was then cooled and the carrier gas was introduced to the reactor. Approximately 1 h was necessary to allow the TCD to stabilize to a linear baseline following changes in carrier gas. After the detector had stabilized, several desorption runs were made to stabilize the surface area of the catalyst and thereby ensure reproducible desorption spectra. Carrier gas flow rates of 20 to 45 cm^3/min were used during adsorption and desorption of H_2. Temperature ramps of 33°C/min were used for all desorption runs. Initial surface coverages of H_2 were varied by changing the number of pulses injected into the carrier gas; in some cases mixtures of less than 10% H_2 were used to obtain low initial coverages. The TCD analysis of H_2 was checked by two methods: (i) experiments in which no hydrogen was adsorbed on catalysts resulted in no TCD signal and (ii) the TPD spectrum for 50% Ni/SiO_2 was reproduced well using the mass spectrometer detector; only H_2 and the carrier gas were detected by the mass spectrometer. Baseline drift was reproducible and was corrected for in the subsequent analysis of the data.

The absence of pore diffusional effects, sample measurement lag time, and concentration gradients within each catalyst particle during the desorption rate measurements was established according to the

criteria of Gorte (*17*). In addition, calculations were performed as suggested by Ibok and Ollis (*18*) which revealed no significant intraparticle diffusion gradients to be present under the conditions used in this study. Concentration gradients in the relatively thin beds (2–8 mm) were small as indicated by a lower than unity value ($<10^{-2}$) of the rate of H_2 desorption relative to the rate of flow leaving the cell. That is, since the instantaneous addition of H_2 to the gas phase at the front, middle, or any other part of the bed was slow relative to the gas flow out of the cell, it follows that the concentration gradient across the bed was small (less than 1%) at any instant during the experiment. Further evidence of small concentration gradients was that the peak temperature was relatively independent of flow rate under the conditions of this study.

Heats of adsorption of H_2 on the Ni/SiO_2 catalysts were determined using the method of desorption rate isotherms (*10, 11, 19*) with corrections for readsorption according to Lee and Schwarz (*11*). A series of 6–10 desorption spectra were obtained with initial coverages ranging from 10 to 100%. Initial coverage was defined as in previous studies (*11, 19*) as the ratio of the area under the entire TPD curve at less than saturation coverage to that at saturation coverage. Desorption isotherms were then plotted as ln (desorption rate) versus $\ln(\theta/1-\theta)$ according to the equation

$$-\frac{d\theta}{dT} = \frac{F}{V_s V_m \beta}\frac{\nu_d}{\nu_a}\left(\frac{\theta}{1-\theta}\right)^2 \exp(-\Delta H_a/RT) \quad (1)$$

where θ is fractional coverage, F is the carrier gas flow rate in cm^3/min, V_s is the volume of solid catalyst, V_m the amount of H_2 adsorbed at full coverage per unit volume of solid catalyst (V_sV_m is the amount of H_2 adsorbed in cm^3), β is the heating rate (33°C/min in this study), ν_a and ν_d are frequency factors for adsorption and desorption, R is the gas constant, T is the temperature in K, and ΔH_a is the enthalpy of adsorption. At fixed values of coverage θ, desorption rates and temperatures were obtained from the desorption rate isotherms. The rate–temperature data thus obtained were then plotted in Arrhenius form. Heats of adsorption were determined for fixed values of coverage from the slopes of Arrhenius plots.

Heats of adsorption were also estimated from the temperature of the desorption rate maximum as outlined for second order desorption kinetics by Konvalinka and coworkers (*14, 20*) using the relation

$$2\ln T_m - \ln\beta = \frac{\Delta H_a}{RT_m} + \ln\left(\frac{(1-\theta_m)^3 V_s V_m \Delta H_a}{2\theta_m FRA^*}\right) \quad (2)$$

where all variables are defined as in Eq. (1) and where T_m is the temperature of peak maximum and θ_m is the coverage at peak maximum. The preexponential factor A^* was found from $A^* = \exp(\Delta S^\circ/R)$ where ΔS° is the standard entropy of gaseous H_2 at the temperature of the peak maximum (*14, 20*).

RESULTS

Figures 1–7 show typical H_2 desorption curves for each of the catalysts tested in this study. The desorption spectra for unsupported Ni powder and 3 and 10% Ni/SiO_2 catalysts in Ar carrier gas (Figs. 1–3) are very similar in that they show only one prominent desorption peak and similar peak maximum temperatures. In contrast, the desorption spectra for 50% Ni/SiO_2, 14% Ni/Al_2O_3, and 10% Ni/TiO_2 (Figs. 4–6) in Ar carrier gas consist of two desorption peaks.

The temperatures of the desorption peak maxima following adsorption at 25°C are listed in Table 1. It is apparent that the desorption curves are shifted to higher temperatures when N_2 is used as the carrier gas compared to He and Ar. Use of N_2 as a carrier gas also results in the appearance of two desorption peaks for 10% Ni/SiO_2 (see Fig. 3). These effects were apparently due

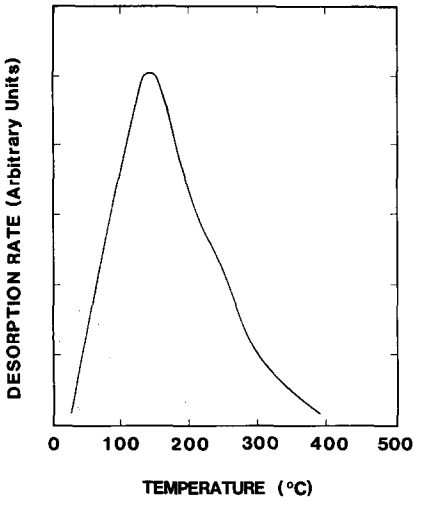

FIG. 1. TPD spectrum for H_2 desorption from unsupported nickel powder (25 cm^3/min of argon carrier gas).

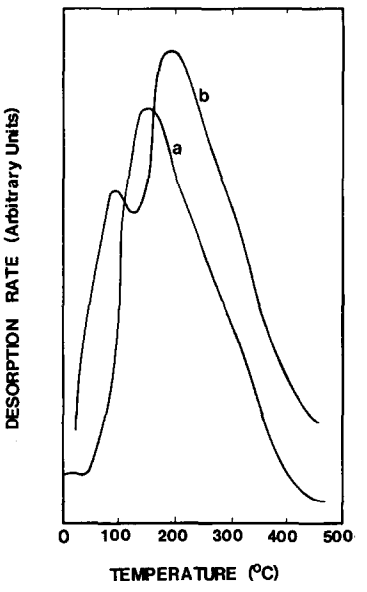

FIG. 3. Hydrogen TPD spectra for 10% Ni/SiO_2: (a) 20 cm^3/min argon carrier gas; (b) 45 cm^3/min N_2 carrier gas.

to the change in carrier gas and were not due to a change in carrier gas flow rate, since a threefold variation in carrier gas flow rate produced negligible changes in peak shape or in the location of desorption peak maxima.

For a given carrier gas, the data in Table 1 provide evidence of significant shifts in desorption peak temperatures with changes in support. For example, there is clearly a shift to higher peak temperature in the order Ni/SiO_2, Ni/TiO_2, Ni/Al_2O_3.

Figures 2, 5, and 7 show the TPD spectra for 3% Ni/SiO_2, 14% Ni/Al_2O_3, and 10% Ni/TiO_2 as a function of the adsorption temperature. Decreasing adsorption capac-

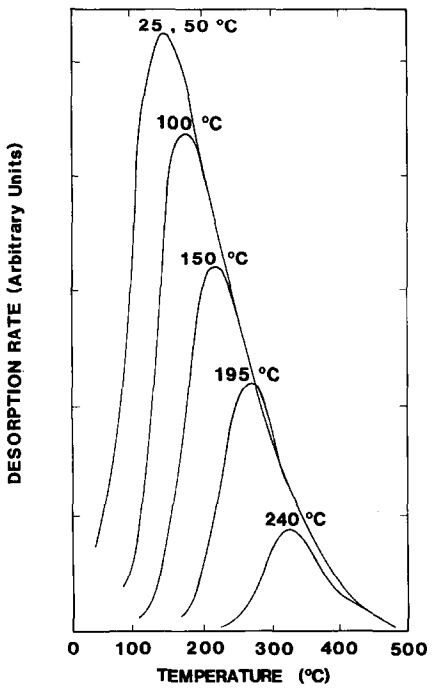

FIG. 2. Hydrogen TPD spectra for 3% Ni/SiO_2 at different adsorption temperatures (30 cm^3/min of argon carrier gas).

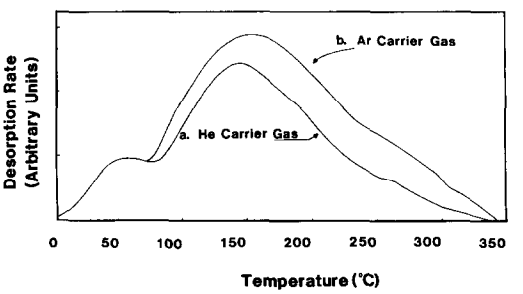

FIG. 4. Hydrogen TPD spectra for 50% Ni/SiO_2: (a) 30 cm^3/min argon carrier gas; (b) 30 cm^3/min He carrier gas.

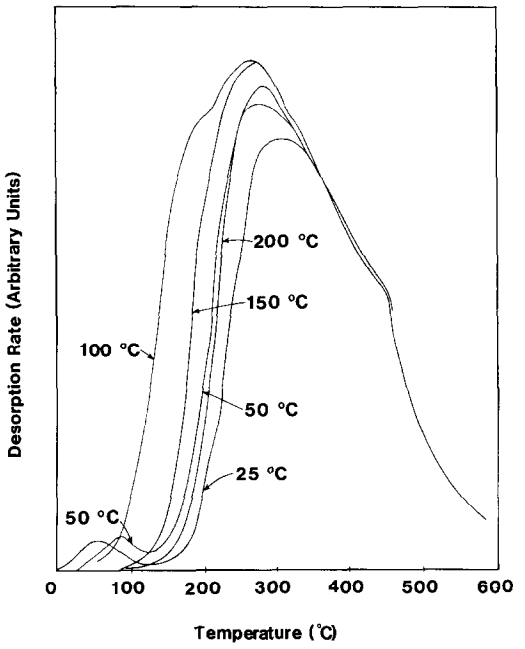

FIG. 5. Hydrogen TPD spectra for 14% Ni/Al_2O_3 at different adsorption temperatures (20 cm^3/min of Ar carrier gas).

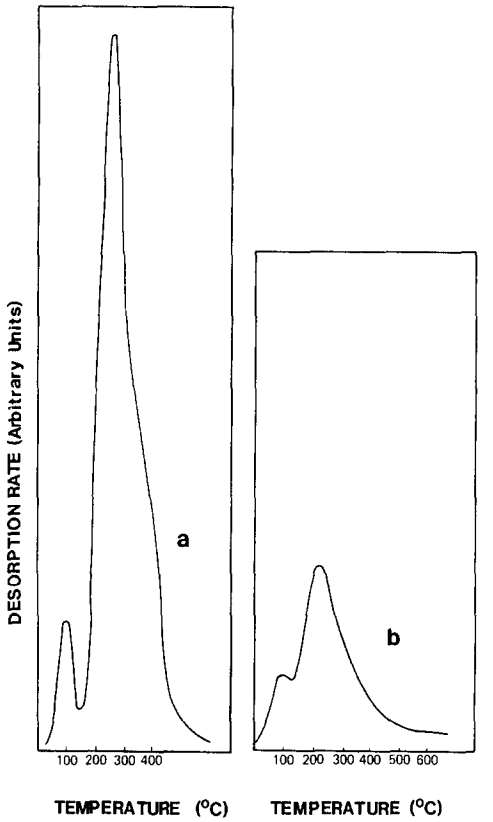

FIG. 6. Hydrogen TPD spectra for 10% Ni/TiO_2 (20 cm^3/min of Ar): (a) After reduction at 400°C; (b) After successive reductions of 1 h each at 400, 500, 600, and 700°C; desorption rates are on the same scale for both runs.

ity with increasing adsorption temperature is evident for the Ni/SiO_2 and Ni/TiO_2 catalysts. However, the amount of H_2 adsorbed on the Ni/Al_2O_3 catalyst increases with increasing temperature, the maximum adsorption occurring between 100 and 150°C. Using the approach of Schwarz *et al.* (*10, 11*) and the experimental method of Zowtiak and Bartholomew (*21*) the activation energy of adsorption was found to be 10 kJ/mole for the Al_2O_3-supported catalyst and approximately zero for the remaining catalysts.

Reduction of the SiO_2- and Al_2O_3-supported catalysts at temperatures of 600 to 700°C for 1 h did not significantly sinter the catalyst or change the desorption spectra from those shown in Figs. 1–5. However, the reduction temperature significantly influenced the spectral shape and area in the case of the Ni/TiO_2 catalyst (See Figs. 6 and 7 and Table 2). Indeed, as the reduction temperature was increased, peak area was significantly decreased and the ratio of the area of the low-temperature peak to that of the high-temperature peak was increased (Table 2). After reduction for 1 h at 600 or 700°C, the peak maximum was shifted to

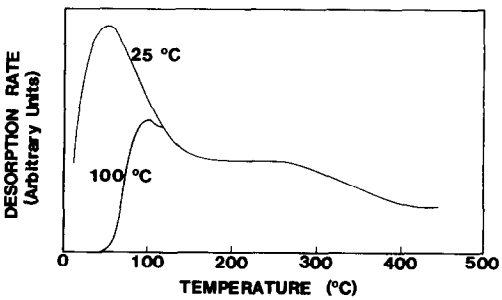

FIG. 7. TPD spectra for H_2 adsorbed on 10% Ni/TiO_2 at 25 and 100°C after high-temperature reduction at 600°C for 16 h (20 cm^3/min of Ar carrier gas).

TABLE 1

H_2 Adsorption Uptakes and Temperatures of Desorption Rate Maximum for Temperature-Programmed Desorption of H_2[a] from Nickel Catalysts

Catalyst	H_2 uptake[b] (μmole/g)	Temperatures of desorption rate maximum, °C		
		Ar	He	N_2
Unsupported Ni	5	135	—	—
3% Ni/SiO_2	100	135		175
10% Ni/SiO_2	370	140		185
50% Ni/SiO_2	800	145	145	200
10% Ni/TiO_2	25 ± 0.5	100		160
		245		290
14% Ni/Al_2O_3	150	60		80
		330		335

[a] After adsorption to saturation coverage at 25°C using the pulse-flow adsorption technique. Temp. in °C.
[b] Total H_2 uptake measured at 25°C by static, volumetric adsorption (Refs. (*3*, *15*)).

lower temperature and the area of the high-temperature peak was markedly reduced (see Fig. 6). After reduction at 600°C for 16 h, only one low-temperature peak of relatively low area was observed (see Fig. 7).

Desorption spectra for 50% Ni/SiO_2 were obtained as a function of initial H_2 coverage. Treatment of these data by the method of desorption rate isotherms (*10*, *11*, *19*, *21*) resulted in plots of ln (rate) versus $\ln[\theta/(1-\theta)]$ having slopes of 2 over wide ranges of temperature and coverage, characteristic of a second-order desorption process. From the desorption isotherms, rates were determined as a function of temperature at fixed values of θ and were plotted in Arrhenius form. Heats of adsorption obtained from the Arrhenius plots are shown in Fig. 8 as a function of coverage. A value of 87 kJ/mole was obtained at low coverage ($\theta = 0.10$) in the He carrier gas (100 kJ/mole in N_2 carrier gas at $\theta = 0.20$). Similar runs involving the 10% Ni/SiO_2 catalyst resulted in a heat of adsorption of 88 kJ/mole at $\theta = 0.20$. Because of uncertainties in the shapes of the nonlinear heats of adsorption versus coverage curves at $\theta < 0.1$–0.2, the data were not extrapolated to zero coverage. Nevertheless, it is clear from the data in Fig. 8 that the value of $-\Delta H_a$ at $\theta = 0.1$–0.2 should be within 2–10 kJ/mole of the value at zero coverage.

Surface areas for the 3% Ni/SiO_2 were too low to obtain accurate desorption isotherms at low coverages. Since the desorption of H_2 from either Ni/Al_2O_3 or Ni/TiO_2 involved overlapping peaks and was incomplete at 500°C (see Figs. 5 and 6) accurate

TABLE 2

Desorption Peak Maxima and Peak Areas for 10% Ni/TiO_2 as a Function of Reduction Temperature (20 cm^3/min of Ar Carrier Gas)

Reduction[a] temp (°C)	Temperature of peak maxima (°C)	Peak areas (Arbitrary units)	Total peak area (Arbitrary units)
400	100	23	285
	245	262	
500	110	26	181
	250	155	
600	100	19	109
	245	90	
700	95	9[b]	75
	200	66	

[a] Sample was reduced successively in flowing H_2 for 1 h at the temperatures shown.
[b] A high degree of peak overlap inhibited accurate determination of peak areas (see Fig. 6b).

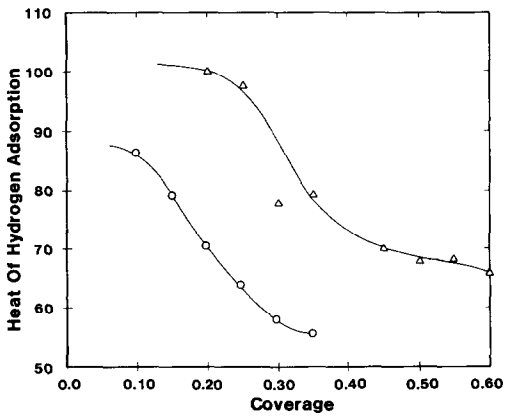

FIG. 8. Heats of hydrogen adsorption on 50% Ni/SiO_2 versus coverage: ○, He carrier gas; △, N_2 carrier gas.

TABLE 3

Heats of Hydrogen Adsorption for Nickel Catalysts Estimated [a,b] from Desorption Peak Temperatures[c]

Catalyst	T_m[d] (°C)	θ_m[e]	$V_s V_m$[f]	A^*[g] ($\times 10^{-6}$)	F[h]	$-\Delta H_a$[i] (kJ/mole)
Unsupported Ni	135	0.48	0.010	17.33	25	87
3% Ni/SiO_2	135	0.48	0.050	17.33	30	82
10% Ni/SiO_2	140	0.48	0.11	18.10	45	82
50% Ni/SiO_2	150	0.48	0.15	19.67	45	84
10% Ni/TiO_2	245	0.48	0.10	39.80	20	105
	100	0.48	0.010	12.70	20	78
14% Ni/Al_2O_3	330	0.49	0.10	67.57	20	125
	60	0.48	0.0050	8.55	20	70

[a] Method of Konvalinka *et al.* (*20*).
[b] Based on a heating rate of 33°C/min.
[c] Peak temperatures measured in Ar carrier gas (Table 1).
[d] Temperature of desorption rate maximum.
[e] Fractional coverage at the maximum peak temperature.
[f] The amount of H_2 adsorbed in cm^3.
[g] The preexponential factor estimated from $\Delta S°$ ($A^* = \exp[\Delta S°/R]$). Values of $\Delta S°$ of 31.00, 32.98, 34.53, and 35.79 at 300, 400, 500, and 600 K, respectively, were taken from Ref. (*14*).
[h] Carrier gas flow rate in cm^3/min.
[i] Heat of hydrogen adsorption in kJ/mole.

measurements of the surface coverage were not possible. As a result, attempts to use the desorption rate isotherm method on these catalysts were unsuccessful. In addition, because the area under the TPD curve was so sensitive to the thermal history of the catalyst (i.e., reduction temperature and time) it was not possible to obtain reproducible quantitative results for Ni/TiO_2.

Estimates of the heats of adsorption from peak temperatures according to the method of Konvalinka *et al.* (*20*) are shown in Table 3 for all of the catalysts tested. The heats of adsorption range from a low of 82 kJ/mole for the Ni/SiO_2 catalyst to a high of 125 kJ/mole for the Ni/Al_2O_3 catalyst. Heats of adsorption estimated from peak temperatures obtained in N_2 carrier gas were generally 10–12% higher than the values shown in Table 3 for the Ar carrier gas.

DISCUSSION

Absence of Diffusional Limitations and Shifts in Desorption Temperature

Quantitative evaluation of data from TPD studies of supported catalysts requires that transport effects be carefully considered. Lee and Schwarz (*11*) concluded that there were no intraparticle diffusion effects or external mass transfer effects using the identical 50% Ni/SiO_2 catalyst under nearly the same flow conditions as existed in this study. The excellent agreement of our heat of adsorption data with theirs for this catalyst (Table 4) strongly suggests that diffusional and transport effects were likewise absent in this study. Moreover, calculations based on criteria proposed by Gorte (*17*) and Ibok and Ollis (*18*) indicate that intraparticle concentration gradients were negligible under the conditions of this study.

Rieck and Bell (*22*) modeled thermal desorption in a porous catalyst bed as a series of constant stirred tank reactors (CSTR) connected in series. Evaluation of our TPD experiments according to their model indicates that the catalyst bed in most of our experiments simulated a single CSTR. In a few experiments involving very low surface area catalysts and relatively long beds, the

TABLE 4

Heats of Adsorption of Hydrogen on Nickel Surfaces

Surface	$-\Delta H_a$ (kJ/mole)	Reference
Ni(100)	97	*26, 27*
Ni(110)	85	*26, 27*
Ni(111)	90	*26, 27*
	95	
Ni(100)	96	*29*
Ni(110)	90	*29*
Ni(111)	96	*29*
Ni(110)	98	*28*
Ni(110)-α	96	*25*
-β	123	*25*
Polycrystalline Ni	83–100	*12*
24% Ni/SiO_2	61, 85, 123	*14*
50% Ni/SiO_2	89[a]	*11*
50% Ni/SiO_2	87[b]	This study
10% Ni/SiO_2	88[c]	This study

[a] At zero coverage using desorption rate isotherms.
[b] At a coverage of 10% using desorption rate isotherms (see Fig. 8).
[c] At a coverage of 20% using desorption rate isotherms.

system was better modeled by a series of two or three CSTR reactors at most. The model of Rieck and Bell predicts a small shift in peak position for the latter case. However, this shift is expected to be only a few degrees centigrade.

While readsorption undoubtedly occurred under the conditions of this study, it was nevertheless taken into account, since the method of desorption rate isotherms used in this and earlier studies (*11, 21*) assumed that readsorption occurred freely. Shifts in the desorption temperature due to readsorption as predicted by Gorte (*17*) and Herz *et al.* (*23*) were relatively small. Indeed, the peak desorption temperatures for unsupported Ni, 3% Ni/SiO_2, and 10% Ni/SiO_2 in the argon carrier were the same within experimental error while that for 50% Ni/SiO_2 was only 5–10°C higher and thus nearly the same (see Table 1). Finally, the fact that heats of H_2 adsorption obtained for the Ni/SiO_2 catalysts in this study were in close agreement with those determined in studies of polycrystalline and single crystal nickel (*12, 24–30*) is further indication that the data were obtained under conditions free of mass transfer disguises.

The heats of adsorption obtained by the method of desorption rate isotherms vary considerably with coverage, e.g., from 55 kJ at $\theta = 0.4$ to 87 kJ at $\theta = 0.1$ for 50% Ni/SiO_2 (see Fig. 8). Thus, the agreement between the heats of adsorption obtained for 10 and 50% in Ni/SiO_2 from temperatures of maximum desorption rate according to Konvalinka *et al.* (*14, 20*) at a coverage of approximately 50% and those obtained at low coverage ($\theta = 0.1$ and 0.2) by the desorption rate isotherm method is unexpected. Since heats of adsorption determined from peak temperatures are sensitive to the assumed value of $\Delta S°$, they are probably more useful as qualitative estimates for relative comparison among a group of catalysts such as in Table 3 than as quantitative numbers for comparison with values determined by other methods.

Effects of Carrier Gas on H_2 Desorption Kinetics

The data obtained in this study provide evidence that desorption kinetics (i.e., TPD peak shapes and position) and heats of adsorption determined from TPD curves are influenced by the choice of carrier gas (see Table 1, Figs. 3 and 8). These effects (increases in peak temperature and heat of adsorption) were most evident in the runs involving N_2 as a carrier gas while the kinetic data obtained in Ar and He were the same within experimental error (Table 1, Fig. 4). Effects of inert gas diluents on the kinetics of CO desorption from graphite were observed by Brown *et al.* (*31*). These effects were attributed to changes in the surface diffusion process with changes in carrier gas which could affect the surface translational entropy, frequency factor, and activation energy for surface migration (*31*). The very close agreement of our results obtained in Ar and He carriers suggests that surface diffusional effects were not important factors in our desorption experiments. The effects observed in the case of the N_2 carrier, are more likely due to the presence of chemisorbed N_2 (*12*), which could conceivably influence the hydrogen atom surface diffusion, recombination, and desorption processes. Argon and helium, on the other hand, should not be chemisorbed on the surface.

Effects of Support on H_2 Adsorption

The data obtained in this study provide evidence that catalyst supports can greatly influence the adsorption states and desorption kinetics for hydrogen/nickel. For example, H_2 desorption data for Ni/Al_2O_3 and Ni/TiO_2 (Table 1 and Figs. 5 and 6) reveal the presence of two new principal adsorption states for H_2 at high temperatures compared to one principal state for unsupported nickel and Ni/SiO_2 (Figs. 1 and 2). Although hydrogen adsorption on Ni/SiO_2 catalysts (*11*) and single crystal nickel (*25–30*) typically involves a low activation barrier, the results of this study show that adsorption of

H_2 on Ni/Al_2O_3 is relatively highly activated. The results of this investigation also provide evidence demonstrating that metal–support interactions can increase the strength of the hydrogen–nickel bond; however, they apparently suppress adsorption of hydrogen in the case of high-temperature-reduced Ni/TiO_2. Each of these phenomena is discussed in more detail below.

New H_2 adsorption states on supported nickel. The type and population of H_2 adsorption sites on Ni is apparently not a strong function of the surface geometry (*11, 25–30*) since the heats of adsorption of H_2 on Ni (100), (110), and (111) at low coverage ($\theta < 0.5$) are the same (93 ± 5 kJ/mole) within experimental error (see Table 4). It should be noted, however, that H_2 adsorbed on the (110) plane in the α-state ($-\Delta H$ = 96 kJ/mole) can slowly transform into a more strongly bound β-state ($-\Delta H$ = 123 kJ/mole) (*14, 25*). Based on the data from this (Fig. 1 and Table 3) and previous studies (*12, 24, 32*) hydrogen apparently adsorbs on unsupported polycrystalline nickel predominantly in the α-state with a heat of adsorption of 85–100 kJ/mole. Adsorption of H_2 on Ni/SiO_2 at low to moderate coverages (θ = 0–0.5) also occurs principally in the α-state ($-\Delta H$ = 82–90 kJ/mole) (see Figs. 2–4 and Table 4) over a wide range of nickel loadings (3–50%). At high coverages ($\theta \cong 1$) obtained by cooling in H_2 from 450°C the TPD spectrum is significantly more complex and may involve as many as 5–6 different adsorption states having a range of adsorption heats from 36 to 170 kJ/mole (*14*); unfortunately the assignment of different states in this case is difficult and arbitrary. Moreover, the importance of the very weakly bound states (−65°C) and strongly bound states (450–475°C) (*14*) in typical catalytic reactions is questionable. Accordingly, the TPD data obtained for the α-state in this and a previous study (*11*) are probably more pertinent to hydrogen adsorption on Ni/SiO_2 under typical reaction conditions.

While hydrogen adsorption on Ni/SiO_2 occurs mainly in the α-state as it does on unsupported polycrystalline or single crystal nickel, two new adsorption states at relatively low (60–100°C) and high (245–330°C) temperatures are observed in the case of Ni supported on Al_2O_3 and TiO_2 (see Tables 1–3 and Figs. 5 and 6). These new states have energies which are clearly different than the α-state of hydrogen bound to unsupported Ni and Ni/SiO_2. Indeed, the high-temperature states for Ni/Al_2O_3 and Ni/TiO_2, which are clearly of interest in CO hydrogenation involve binding energies ($-\Delta H$ = 104–123 kJ/mole) more characteristic of the β-state on Ni (110). These new states may result from electronic modifications of small nickel crystallites present in these catalysts which interact intimately with the support (*33*).

Activated H_2 adsorption. Adsorption of hydrogen on nickel is generally assumed to be nonactivated (i.e., to have a zero activation energy) (*34*). Indeed, Roberts (*35*) observed an activation energy for adsorption of H_2 on nickel wire of only 1.7 kJ/mole. Moreover, the kinetics of adsorption/desorption from H_2 on single crystal nickel (*25–30*) are consistent with this assumption. This work and that by Lee and Schwarz (*11*) show that hydrogen adsorption on Ni/SiO_2 is very weakly activated; indeed, the amount adsorbed decreases with increasing temperature (see Fig. 2) as would be expected if the rates of adsorption and desorption were close to equilibrium. However, the data of this study show that H_2 adsorption on Ni/Al_2O_3 is more strongly activated (E_a = 10 kJ/mole). Indeed, the amount of H_2 adsorbed increases with increasing temperature from 25 to 200°C (see Fig. 5), indicating that the rate of adsorption increases to a greater extent than the rate of desorption with increasing temperature. Previous studies have demonstrated that hydrogen adsorption on cobalt is activated (*36–39*), and recent studies in this laboratory (*21, 39*) have shown that the degree of activation is strongly dependent on support and cobalt metal loading.

Suppression of H_2 adsorption on Ni/TiO_2. Previous static adsorption studies (*2–5*) demonstrated that H_2 adsorption is suppressed at low loadings in Ni/Al_2O_3 and at moderate loadings in Ni/TiO_2, the extent of which is determined in part by reduction temperature (*3*). TPD data obtained for Ni/TiO_2 in this study (Table 2 and Figs. 6 and 7) show significant decreases in adsorption capacity and a shift to lower desorption peak temperature with increasing reduction temperature.

Ko and Winston (*40*) investigated effects of nickel metal loading and crystallite size on the onset of strong metal support interactions (SMSI) for Ni/TiO_2 systems. Using suppression of H_2 chemisorption and ethane hydrogenolysis as probes they reported that SMSI did not occur until high reduction temperatures (e.g., >500°C) were reached in the case of 5–10% Ni/TiO_2. At lower metal loadings, e.g., 2%, SMSI effects were observed at lower reduction temperatures (e.g., 300°C). In the SMSI state they observed that hydrogen chemisorption and ethane hydrogenolysis were significantly suppressed while X-ray diffraction and electron microscopy revealed no significant loss of metal surface area.

Our results are qualitatively in agreement with those of Ko and Winston. Indeed, we observed significant suppression of H_2 adsorption on 3% Ni/TiO_2 at reduction temperatures lower than those for the corresponding effects in 10% Ni/TiO_2. Moreover, our results clearly show a very significant suppression of H_2 adsorption on 10% Ni/TiO_2 for reduction temperatures above 500°C. In addition, our study provides new evidence that the SMSI state of Ni on titania involves a much lower binding energy for H_2 relative to the states observed after low-temperature reduction. This is consistent with recently obtained calorimetric data (*41*) showing that the heat of adsorption of H_2 on Ni/TiO_2 reduced at high temperature is significantly lower than for the same catalyst reduced at low temperature.

CONCLUSIONS

1. The number and relative occupancy of hydrogen adsorption states at moderate to low coverages and heats of adsorption of hydrogen on nickel are affected significantly by the support. For example, heats of H_2 adsorption on unsupported Ni and Ni/SiO_2 are about 90 kJ/mole whereas that for H_2 on Ni/Al_2O_3 is 122 kJ/mole.

2. Hydrogen adsorption on Ni/Al_2O_3 is an activated process, i.e., the uptake increases with increasing temperature and reaches a maximum at a temperature of 100°C. Hydrogen adsorption on unsupported Ni, Ni/SiO_2, and Ni/TiO_2 involves a low activation barrier, i.e., the adsorption process is rapid and the amount adsorbed decreases with increasing temperature.

3. Hydrogen adsorption on Ni/TiO_2 is strongly suppressed by reduction at high temperature. Moreover, there is a shift with increasing reduction temperature in relative occupancy from a high-temperature state to a low-temperature state of lower binding energy.

4. The presence of N_2 carrier gas alters TPD spectra from those obtained using He or Ar carrier gases, i.e., peak temperatures and heats of adsorption are higher in N_2 atmosphere. This effect may be due to adsorption of N_2 on the nickel surface.

ACKNOWLEDGMENTS

The authors gratefully acknowledge support from the National Science Foundation (Grant CPE-7910823), technical assistance by Mr. John M. Zowtiak, and the gift of a sample of 50% Ni/SiO_2 by Dr. James L. Carter of Exxon Research and Engineering.

REFERENCES

1. O'Neill, C. E., and Yates, D. J. C., *J. Phys. Chem.* **65,** 901 (1961).
2. Vannice, M. A., and Garten, R. L., *J. Catal.* **56,** 236 (1979).
3. Bartholomew, C. H., Pannell, R. B., and Butler, J. L., *J. Catal.* **65,** 335 (1980).
4. Bartholomew, C. H., Pannell, R. B., Butler, J. L., and Mustard, D. G., *I & EC Prod. Res. Dev.* **20,** 296 (1981).

5. Smith, J. S., Thrower, P. A., and Vannice, M. A., *J. Catal.* **68,** 270 (1981).
6. Zagli, A. E., Falconer, J. L., and Keenan, C. A., *J. Catal.* **56,** 453 (1979).
7. Falconer, J. L., and Zagli, A. E., *J. Catal.* **62,** 280 (1980).
8. Cvetanovic, R. J., and Amenomiya, Y., "Advances in Catalysis," Vol. 17, p. 102. Academic Press, New York, 1967.
9. Cvetanovic, R. J., and Amenomiya, Y., *Catal. Rev.* **6**(1), 21 (1972).
10. Falconer, J. L., and Schwarz, J. A., *Catal. Rev.-Sci.-Eng.* **25**(2), 141 (1983).
11. Lee, P. I., and Schwarz, J. A., *J. Catal.* **73,** 272 (1982).
12. Toyoshima, I., and Somorjai, G. A., *Catal. Rev.-Sci.-Eng.* **19,** 105 (1979).
13. Popora, N. M., Babenkova, L. V., and Sokol'skii, *Kinet. Katal.* **10,** 1171 (1969).
14. Konvalinka, J. A., Van Oeffelt, P. H., and Scholten, J. J. F., *Appl. Catal.* **1,** 141 (1981).
15. Bartholomew, C. H. and Farrauto, R. J., *J. Catal.* **45,** 41 (1976).
16. Weatherbee, G. D., and Bartholomew, C. H., *J. Catal.* **68,** 67 (1981).
17. Gorte, R. J., *J. Catal.* **75,** 164 (1982).
18. Ibok, E. E., and Ollis, D. F., *J. Catal.* **66,** 391 (1980).
19. Falconer, J. L., and Madix, R. J., *J. Catal.* **48,** 262 (1977).
20. Konvalinka, J. A., Scholten, J. J. F., and Rasser, J. C., *J. Catal.* **48,** 365 (1977).
21. Zowtiak, J. M., and Bartholomew, C. H., *J. Catal.* **83,** 107 (1983).
22. Rieck, J. S., and Bell, A. T., *J. Catal.* **85,** 143 (1984).
23. Herz, R. K., Kiela, J. B., and Marin, S. P., *J. Catal.* **73,** 66 (1982).
24. Sweet, F., and Rideal, E., "Actes du Deuxieme Congres International de Catalyse, Paris, 1960," p. 175. Editions Technip, Paris, 1961.
25. Ertl, G., and Kuppers, D., *Ber. Bunsenges. Phys. Chem.* **75,** 1017 (1971).
26. Lapujoulade, J., and Neil, K. S., *Surf. Sci.* **35,** 288 (1972).
27. Lapujoulade, J., and Neil, K. S., *J. Chem. Phys.* **70,** 798 (1973).
28. McCarty, J., Falconer, J., and Madix, R. J., *J. Catal.* **30,** 235 (1973).
29. Christmann, K., Schober, O., Ertl, G., and Neumann, M., *J. Chem. Phys.* **60,** 4528 (1974).
30. Christmann, K., *Z. Naturforsch. A* **34,** 22 (1979).
31. Brown, L. F., Britten, J. A., and Falconer, J. L., "183rd ACS National Meeting," Las Vegas, Nevada, April 2, 1982.
32. Wedler, G., "Chemisorption: An Experimental Approach." Butterworths, London, 1976.
33. Kao, C.-C., Tsai, S.-C., and Chung, Y.-W., *J. Catal.* **73,** 136 (1982).
34. Clark, A., "The Theory of Adsorption and Catalysis," p. 211. Academic Press, New York, 1970.
35. Roberts, J. K., *Proc. Roy Soc. (London), Ser. A.* **152,** 445 (1935).
36. Matsumura, S., Tarama, K., and Kodema, J., *J. Soc. Chem. Ind. (Jpn.)* **43,** 175 (1940), Suppl. Binding.
37. Sastri, M. V. C., and Srinivasan, V., *J. Phys. Chem.* **59,** 503 (1955).
38. Dollimore, J., and Harrison, B., *J. Catal.* **28,** 275 (1973).
39. Zowtiak, J. M., Weatherbee, G. D., and Bartholomew, C. H., *J. Catal.* **82,** 230 (1983).
40. Ko, E. I., and Winston, S., *Roy. Soc. Chem. Commun.* (**13**), 740 (1982).
41. Vannice, M. A., "DOE Conference on Heterogeneous Catalysis," Gaithersburg, Maryland, November 7–9, 1983.